



The influence of inter-ply friction during double-diaphragm forming of biaxial NCFs

G.D. Lawrence, S. Chen, N.A. Warrior, L.T. Harper*

Composites Research Group, Faculty of Engineering, University of Nottingham, NG7 2RD, UK

ARTICLE INFO

Keywords:

- A. Fabrics/textiles
- B. NCF
- C. Friction
- E. Forming

ABSTRACT

Inter-ply friction plays an important role in the formation of defects in automated preforming of complex components, as relative sliding between plies can generate local compressive stresses in the direction of the primary yarns, leading to out-of-plane wrinkling and other defects such as fibre buckling and bridging.

This work presents a novel characterisation method for measuring the coefficient of friction at fabric-fabric interfaces, using a set up that can generate inter-ply slip conditions representative of those experienced during double diaphragm forming. Results for a pillar stitched, biaxial NCF indicate the sensitivity of the coefficient of friction to the level of applied compaction pressure generated by the diaphragm. Friction values are observed to be typically 100% higher than those recorded using a conventional sled test (ASTM D1894). Additionally, this behaviour is dependent on the relative fibre orientation at the inter-ply interface, which affects the nesting/compaction behaviour of the plies. This has been confirmed using optical micrographs and through-thickness compaction tests.

The significance of these orientation and pressure dependencies has been studied using a modified hemisphere forming rig to control the degree of inter-ply slip. Results from the test indicate that punch force is dependent on the fibre angles at the inter-ply interface, and that variation in the local friction behaviour can affect the formability of a component and induce unwanted defects.

1. Introduction

To meet sustainability, manufacturing rate and cost demands, autoclave curing of prepregs is shifting towards lower energy processes such as liquid composite moulding, but quality challenges must be addressed. Preforming of binder-stabilised dry fabrics can be automated to meet this demand, using processes such as double diaphragm forming (DDF) [1,2] or matched-tool thermoforming [3], to produce complex 3D preforms. However, these high-rate preforming processes do not typically offer the same level of control over the deformation of the fabric plies compared to highly skilled hand layup operations, commonly resulting in defects for complex components. Consequently, automated preforming processes are currently reserved for relatively simple shapes and ply layouts.

Defects generated during preforming may take the form of fabric wrinkles, laddering or fibre/yarn buckling, and can have a detrimental effect on the mechanical properties of the finished component [4,5]. While the mechanisms that produce these defects differ depending on the forming process and fabric architecture, they are typically

influenced by the tensile, shear, bending and frictional properties of the dry fibrous material [6–9]. The in-plane tensile and shear forming mechanisms are well documented for a large range of fabrics in the literature, however the macroscale frictional behaviour of fibrous materials is less understood.

Inter-ply slip is a key deformation mode that occurs during composite forming, for both dry fibres [10,11] and saturated/pre-impregnated fabrics [12,13]. Furthermore, controlling inter-ply slip by reducing the coefficient of friction (CoF) between the two contacting surfaces can improve the formability of fabric plies over complex surfaces [11,14,15]. A comprehensive understanding of the frictional behaviour of deformable fabric plies is therefore required in order to improve preform quality. This behaviour can be classified across three scales [16]; microscale (individual filament level), mesoscale (tow level) and macroscale (ply level). Whilst the macroscale frictional behaviour is arguably the most relevant for automated preforming processes, it is directly affected by phenomena that occur at the mesoscale, which in turn are affected by the microscale. Accordingly, it is important to take a multi-scaled view when considering friction-based process

* Corresponding author.

E-mail address: lee.harper@nottingham.ac.uk (L.T. Harper).

<https://doi.org/10.1016/j.compositesa.2023.107426>

Received 27 August 2022; Received in revised form 6 December 2022; Accepted 2 January 2023

Available online 4 January 2023

1359-835X/© 2023 The Author(s). Published by Elsevier Ltd. This is an open access article under the CC BY license (<http://creativecommons.org/licenses/by/4.0/>).

modifications.

The frictional behaviour at the inter-ply interfaces is dictated by both the material properties of the fabric and the forming process parameters. The level of inter-ply slip within a multi-ply stack is dependent on the relative ply orientations at the macroscale [10], with the frequency of oscillations in the frictional load–displacement curves dependent on the geometry of the fabric unit cell. Similarly, the frictional behaviour at the micro- and mesoscales is anisotropic, as the inter-filament and inter-tow frictional forces are dependent on the relative fibre angle [17]. Inter-tow angles close to 0° can produce coefficients of friction twice as high as those observed for perpendicular tow contacts at the mesoscale [18], due to a relatively higher tow-to-tow contact area. The structure of the fabric ply at the macroscale is influenced by the organisation of the filaments at the microscale, which is influenced by the level of through-thickness compaction [19]. It has been shown experimentally that changes in the microstructure affects the macroscale frictional behaviour, either by changing the real contact area between plies [16], or by the micro and mesoscale mechanisms by which sliding occurs [20].

A widely used method for characterising the macroscale frictional behaviour is the sled test (ASTM standard D1894-14) [1,21–23]. The test was originally developed for plastic film and sheeting materials but has been adapted to suit fabric specimens. A fabric coupon is fixed to a mass, which is pulled over another stationary fabric coupon at a constant velocity. The pulling force applied to the sled is recorded and a standard Coulomb friction law is used to determine the static and dynamic coefficients of friction for the given surface interaction. The sled test is simple to perform, but a significant disadvantage of the test arrangement is the practical upper limit on the applied normal pressure. The fabric specimens are more sensitive to the applied normal pressure, but it is difficult to balance larger loads on the sled without increasing the footprint. The sled is also reported to experience stick–slip motion [24], producing large and varied oscillations in the resulting data.

The ply pull-through, or pull-out friction test [16,25–30] overcomes many of the drawbacks of the sled test. The pull-through test is typically undertaken by applying relative motion to a central fabric sample, clamped between two additional fabric plies. The outer samples are held in place by rigid, parallel platens that can be heated. A normal load is applied to the central sample using a pneumatic or hydraulic system. The central sample can either be fixed to a support plate to prevent deformation due to tensile and shear forces, or simply allowed to deform. The pull-through test is more versatile than the sled test, as it

provides greater control over test parameters, such as normal load and temperature. However, it requires the use of a custom-built testing rig, and no test standard currently exists. The test is typically performed vertically, which makes it difficult to contain liquid resins if the frictional behaviour of saturated fabrics is of interest.

This paper investigates the inter-ply frictional behaviour of a stitched biaxial non-crimp fabric (NCF), using a novel characterisation method to capture the response of the fabric under diaphragm forming conditions, overcoming the deficiencies of the tests reviewed above. The test configuration uses a pair of overlapped fabric plies within a vacuum bag arrangement, which is loaded into a set of tensile jaws in a universal testing machine. For the current work, the test is used to study the dependency of the inter-ply coefficient of friction for dry fabric plies on the applied normal pressure and the relative fibre orientation at the inter-ply interface. Future work will consider fabric plies saturated with liquid resin.

2. Methodology

2.1. Materials

The primary NCF material used for the experimental study was a polyester pillar stitched biaxial fabric (designated FCIM359), provided by Hexcel Reinforcements, Leicester, UK. The relevant properties of FCIM359 are shown in Table 1. Samples were cut to size using a rotary cutting knife.

A second biaxial NCF was used to study the influence of using a polymer veil material on the inter-ply frictional behaviour. Hexcel HiMax® MBB00 was selected as a comparison to FCIM359, due to a similar biaxial NCF architecture and areal weight. The non-woven thermoplastic polymer veil is commonly included to improve the inter-lamina fracture toughness of the composite. The relevant properties of MBB00 can be found in Table 2.

The vacuum bag material used for the overlap test was VACflexP, a nylon bagging film in a ‘sock’ format (i.e. factory sealed along both edges) typically used for vacuum infusion, which was purchased from VAC Innovation. The properties of the VACflexP film are presented in Table 3.

Inter-ply friction experiments were performed using a range of ply orientations and normal pressures, with the nomenclature described in Table 4. Whilst the FCIM359 fabric is biaxial, only the fibre and stitch

Table 1
Material properties for FCIM359 NCF [39,40].

Name	FCIM359
Supplier	Hexcel
Fabric type	Biaxial NCF
Areal weight	441gsm
Fabric thickness	0.4 mm
Stitching	Polyester pillar stitch, 4.5 mm spacing
Fibre	24 k carbon tows
On-roll fabric orientation	Stitch 0°, fibre ± 45°



Table 2
Material Properties of MBB00 NCF.

Name	HiMax® MBB00		
Supplier	Hexcel		Veiled fabric face
Fabric type	Biaxial NCF		
Areal weight	536gsm		
Fabric thickness	0.52 mm		Non-veiled fabric face
Stitching	Polyester pillar stitch		
Fibre	12 k carbon tows		
On-roll fabric orientation	Stitch 0°, fibre ± 45°		

Table 3
Material properties for VACflexP bagging film.

Name	VacflexP
Thickness	0.05 mm ± 10 %
Density	1.13 gm ⁻³
Tensile strength	95 MPa ± 10 %
Machine direction	
Tensile strength	90 MPa ± 10 %
Transverse direction	
Elongation at break	320 % ± 10 %
Machine direction	
Elongation at break	370 % ± 10 %
Transverse direction	

orientations at the contact surface are considered for the naming convention of the tests. Interfacial fibre angles are used to name each surface interaction according to a clockwise positive direction when viewed from the front face of the test packet (shown as yellow lines in Table 4), relative to the direction of slip (shown as red lines in Table 4). Also relevant to the results of the test are the stitch angles of each of the samples, which are 45° out of phase with the fibre angles (i.e., the stitch angle of the first plate is -45° from the fibre direction and the stitch angle of the second plate is +45° when in contact with each other).

2.2. Overlap friction test

Vacuum pressure is applied normal to the tool surface during double diaphragm forming, which can produce undesirable compressive forces in the fibres and prevent fabric sliding. This out-of-plane compression consolidates the laminate stack and changes the surface topography of the fabric at the contact interfaces. It is difficult to capture these effects using the sled test, therefore a new test has been developed to address this issue and to generate conditions more representative of the forming process.

As with diaphragm forming, the new friction test uses vacuum pressure to produce a normal load over one or more surface interactions. Similar to existing ply pull-through tests, fabric samples are affixed with 3 M double-sided adhesive tape to opposing faces of a pair of rigid support plates (200 × 50 mm), as shown in Fig. 1. The tape covered the entire area of the support plate, rigidly fixing the fabric samples in position. The fabric samples overlap, with an initial contact area of 8750 mm². The support plates are used to isolate the frictional behaviour of

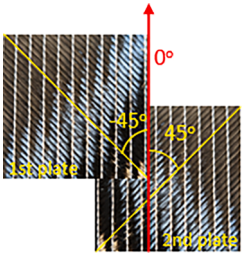
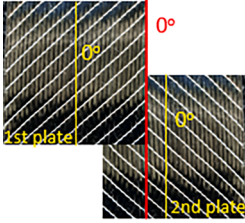
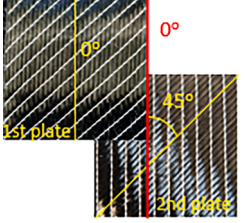
the fabric from the in-plane deformation of the plies, which is particularly important when the fibre orientations are off-axis to the sliding direction. Spacer tabs are used at the ends of the support plates to compensate for the thickness of the fabric plies to ensure the sliding plane is central to the assembly when the plates are clamped in the testing frame, avoiding any unwanted bending.

The support plates containing the fabric plies are loaded into a vacuum bag sock with some breather material, which is sealed at both ends using tacky tape to form a 'test packet' (see Fig. 1b). The test packet is connected to a vacuum pump via a through-bag bayonet fitting and the air is evacuated to simulate the clamping stage of the DDF process. A valve and a pair of digital vacuum gauges are used to regulate the normal clamping load, with a gauge at each end of the bag to ensure the vacuum pressure is uniformly distributed. Fujifilm Prescale pressure measurement film was used to measure the distribution of the vacuum pressure prior to testing. Results indicated that the pressure was uniformly distributed across the entire overlap area.

The test packet is then loaded within rubber-faced tensile jaws attached to 10kN side action grips, as shown in Fig. 1, clamping through the diaphragm material onto the ends of the support plates. The grip faces are the same size as the spacer plates (25x50mm), aiding alignment of the test packer within the universal testing frame. A constant vertical displacement is applied via the crosshead at a velocity of 50 mm/min, extending the test packet and causing the fabric samples to slide over each other. The force required to generate this displacement is recorded via a 50kN load cell. The extension of the test packet was observed to have no effect on the quality of the vacuum applied, as determined by a digital vacuum gauge positioned below the lower clamp. The vacuum gauge and the tacky tape seals at the ends of the vacuum bag were positioned outside of the deformed area, avoiding any influence on the measured frictional force.

Targets placed on the steel support plates were tracked by a video extensometer to validate the crosshead displacement by ensuring there was no additional compliance within the system. The average displacement error between the crosshead data and the video extensometer was 0.16 % over a sliding distance of 50 mm. Multiple pairs of video extensometer targets were used to confirm that the plates slipped linearly with no rotation during the test. The circular targets used to track the displacement were approximately 5 pixels in diameter (0.47 mm), representing a systematic error of 0.93 % in a displacement distance of 540 pixels (50 mm) over the course of the test.

Table 4
Example surface interaction configurations for friction characterisation tests.

Schematic of inter-ply interface	Laminate layup	Nomenclature (fibre angle at inter-ply interface)	Stitch angle at inter-ply interface	Inter-ply fibre orientation
	[+45/-45//+45/-45]	[-45°/45°]	0°/0°	90°
	[90°/0°/0°/90°]	[0°/0°]	-45°/45°	0°
	[90°/0°/+45°/-45°]	[0°/45°]	-45°/0°	45°

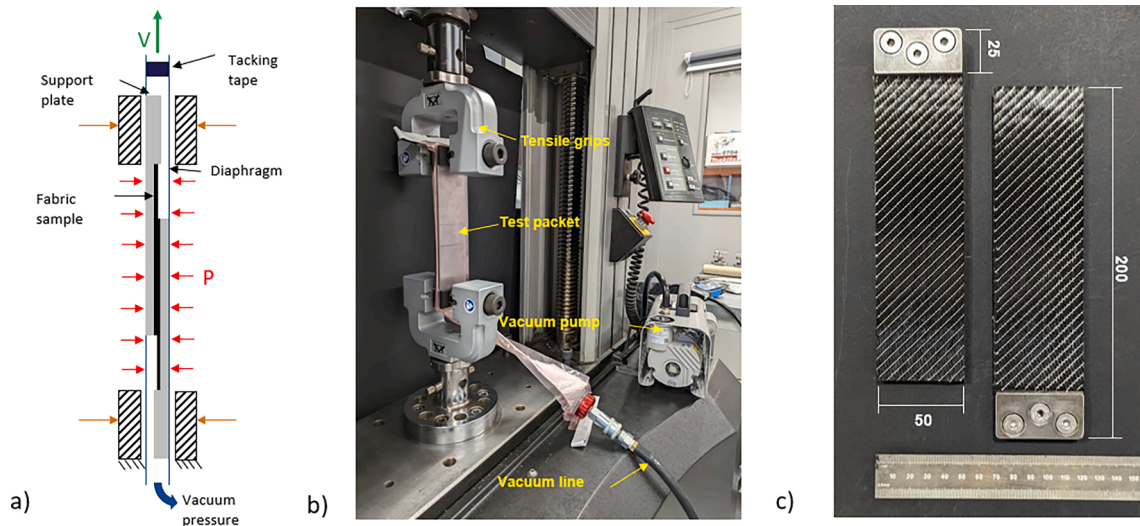


Fig. 1. (a) Schematic of the overlap test. (b) Test packet containing fabric samples and support plates loaded in universal testing frame. Key components of the test are labelled. (c) FCIM359 fabric samples affixed to support plates with dimensions labelled for a [0°/0°] test.

2.3. Calculating the frictional force

The force required to extend the test packet is influenced by not only the friction at the inter-ply contact surface, but also the tensile stiffness of the diaphragm material and additional frictional forces from the surface interactions between the diaphragm and the support plates. It is therefore necessary to process the raw data measured by the load cell to isolate the frictional force of interest at the inter-ply interface. The inter-ply frictional force is established using a calibration curve for a non-deformable material with a known coefficient of friction.

Friction data for non-deformable baseline materials was obtained from a sled test, which was used to calculate a theoretical frictional force over an extension range, using Coulomb’s law of friction ($F = \mu N$). This theoretical friction data was then subtracted from the original crosshead test to determine the unwanted load contribution from the vacuum bag extension and any other interactions within the test packet.

The coefficients of friction were measured for two different non-deformable materials using the overlap test, which were compared to reference values measured by the conventional sled test. Both materials

produced identical calibration curves for the data reduction process when a normal pressure of 1×10^5 Pa was applied. The results from the overlap test for dry steel (CoF of 0.35) and PTFE (CoF of 0.14) were found to be in good agreement with the reference data obtained from the sled test. This confirmed that the unwanted contribution from the stiffness of the vacuum bag and the additional friction surfaces between the bag and the plates could be effectively removed, validating the test setup. If the vacuum pressure, initial contact area and extension distance are kept constant over all experiments, the subsequent calibration curve can be assumed to be constant for any surface pairing.

This data reduction process is described in Fig. 2, indicating results for a steel-steel interaction. The theoretical frictional force curve is calculated from the coefficient of friction obtained from the sled test. This force decreases since the overlap distance decreases with increasing extension (for a given constant applied pressure). No change in coefficient of friction was observed as the applied pressure was increased for the steel-steel interaction, which confirms the robustness of the approach.

Fig. 3 shows the data reduction process applied to a fabric-fabric interaction for a pair of FCIM359 plies. The calibration curve obtained from the steel-steel interaction is used to isolate the frictional force from the crosshead load curve, which is based on an average of 3 repeat specimens. The resulting isolated frictional force decreases, since the applied pressure is constant but the specimen overlap area decreases. This isolated load can subsequently be used to obtain the coefficient of friction for any given extension point.

Fig. 4 shows the variation in coefficient of friction for a pair of FCIM359 plies using the overlap test, determined from the isolated friction load using Coulomb's law. The normal load for every given point of extension is determined using the remaining overlap area of the plates to determine the coefficient of friction ($\mu = \frac{F}{pA}$). Whilst Coulomb's law is a simplification, it is considered to be appropriate for this coupon test because the ratio between the frictional and normal forces is assumed to be constant, producing a steady state value for the dynamic coefficient of friction, $\mu_{dynamic}$ [25], as indicated by the linear portion of the curve in Fig. 4. A large peak can be seen at approximately 2.5 mm of extension, indicating the static coefficient of friction, μ_{static} . Additional information can be derived from the curve that may be useful for future surface interaction modelling, including the static to dynamic decay constant, β [26]:

$$\beta = \frac{\ln\left(\frac{\mu_{static}}{\mu_{dynamic}}\right)}{\Delta x} \quad (1)$$

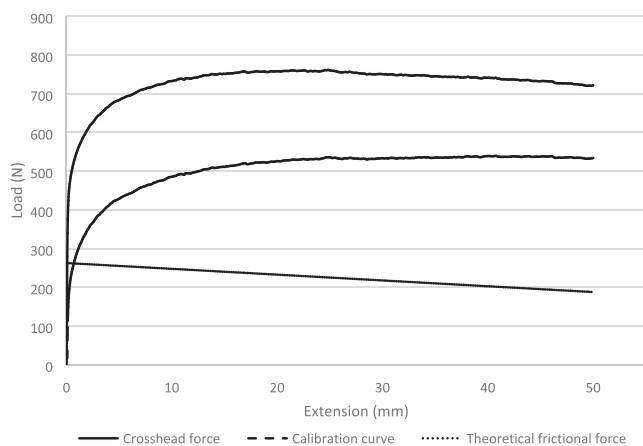


Fig. 2. Data reduction process for a steel-steel interaction using a known friction coefficient of 0.35. The linear theoretical friction is subtracted from the measured crosshead force to produce a calibration curve containing the additional load data that is not of interest.

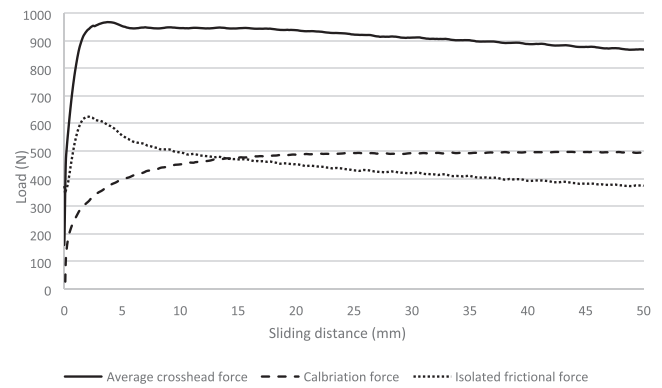


Fig. 3. Data reduction process for an FCIM359 fabric-fabric interaction with an interaction with a parallel fibre orientation ($[-45^\circ/45^\circ]$).

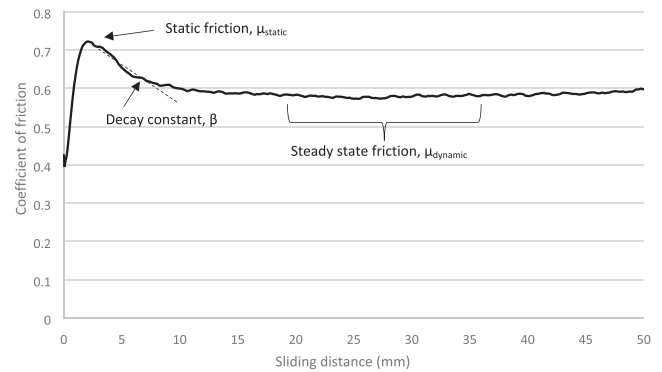


Fig. 4. Variation in coefficients of friction for an FCIM359 fabric-fabric interaction with stitch angles of $[0^\circ/90^\circ]$ and parallel fibre angles of $[-45^\circ/45^\circ]$.

2.4. Fabric compaction tests

Both biaxial fabrics were analysed using a through-thickness compaction test (Fig. 5) fitted to a universal testing machine, to understand the nesting behaviour of the plies. Fabrics with lower through-thickness stiffnesses are more susceptible to fibre nesting about the inter-ply interface and are therefore likely to exhibit higher coefficients of friction.

The test rig used two lateral LVDTs to ensure both parallelism of the upper and lower platens and to eliminate the effect of unwanted compliance within the system. All tests were conducted at a rate of 1 mm/min, as the effect of compaction speed was not investigated for this study. The applied force was measured by a 50kN load cell.

Fabric coupons were cut to 50×50 mm and stacked to create 2, 4, 8 and 10 ply laminates. The ply orientations were chosen to produce parallel, perpendicular and 45° inter-ply fibre orientations for every inter-ply surface interaction through the stack, $[[0^\circ/90^\circ//90^\circ/0^\circ]_{n/2}$, $[0^\circ/90^\circ]_n$ and $[0^\circ/90^\circ//\pm 45^\circ]_{n/2}$ respectively, where n refers to the total number of plies in the layup).

2.5. Hemisphere forming study

A matched tool forming case was used to simulate the effect of different inter-ply sliding conditions within a multi-ply preform, in order to contextualise the friction values obtained from the coupon test. A schematic of the forming set up is shown in Fig. 6(a), demonstrating the inclusion of a vacuum bag to generate a 0.1 MPa clamping pressure on the preform, representative of the DDF process. Fabric samples affixed to aluminium plates (Fig. 6b) were assembled about a central fabric blank to control the local coefficient of friction. Attempts were made to generate areas of high friction to inhibit uniform draw-in of the blank

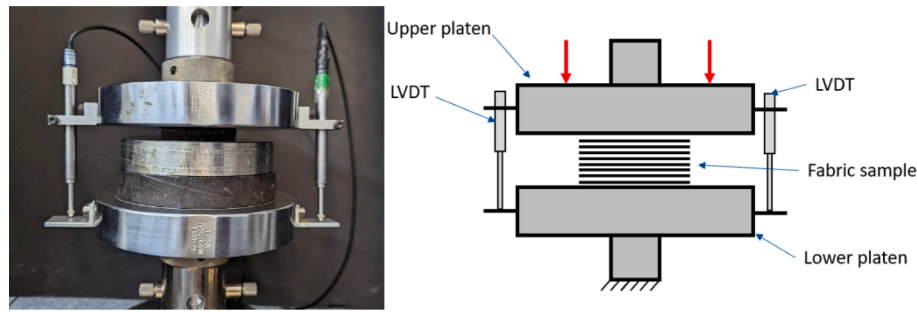


Fig. 5. Schematic of compression test set up, showing bilateral LVDTs to validate the compressive displacement measurement.

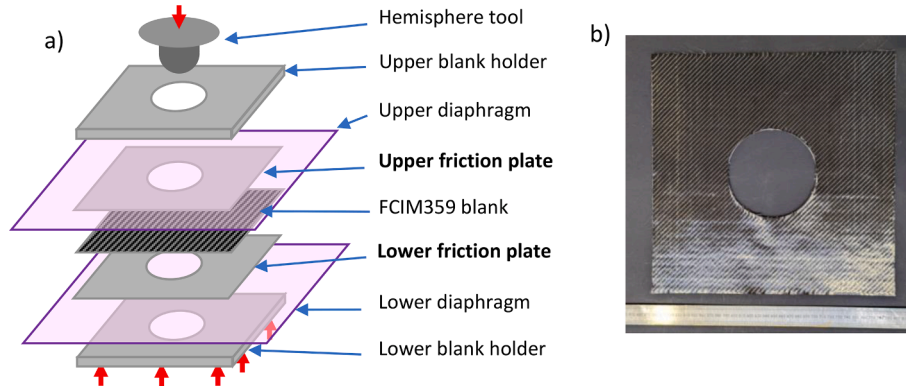


Fig. 6. (a) Schematic of match tool forming test to simulate inter-ply sliding. (b) Friction plate affixed with fabric sample to generate areas of high and low friction.

during the forming process, to create areas of fabric bridging, and to manipulate the shear behaviour in the final preform.

Two 300×300 mm FCIM359 plies were used to produce the preform blank, between which Epikote 05390 powder binder was applied to stabilise the geometry once it had been formed. A layup of $[0^\circ/90^\circ//90^\circ/0^\circ]$ was used to produce the preforms for two reasons: to minimise slip at the interface between the two central plies, and to ensure symmetry of the frictional forces about the midplane of the laminate. The forming process was conducted at ambient temperature to avoid influencing the friction. The hemispherical punch and the blank holders were heated to 100°C once the form was complete, in order to activate the powder binder. The punch force was recorded using a 50kN load cell on a universal testing machine. The force required to deform the vacuum bag was subtracted from the measured punch force to isolate the force required to enable the fabric plies to slip.

3. Results and discussion

3.1. Effect of normal load

Results from the overlap test indicate a pressure dependency for the frictional behaviour of FCIM359. Fig. 7 shows the variation of the coefficient of friction over the 50 mm sliding distance during the overlap test for a range of applied pressures. The surface interaction was $[-45^\circ/-45^\circ]$ in each case. Data were obtained using the sled test for the lowest applied pressure of 4 kPa, producing static and dynamic coefficients of friction of approximately 0.29 and 0.25 respectively. However, both the static and dynamic coefficients of friction are much higher when the fabric plies are subjected to higher normal loads. At 50 kPa (half vacuum pressure) the static and dynamic coefficients were found to be 0.50 and 0.38 respectively. These values increased further to 0.55 and 0.48 at an applied pressure of 75 kPa, and to 0.73 and 0.58 at full vacuum pressure (100 kPa). An increase of 60 % is therefore observed for the static coefficient of friction and 57 % for the dynamic coefficient of friction when

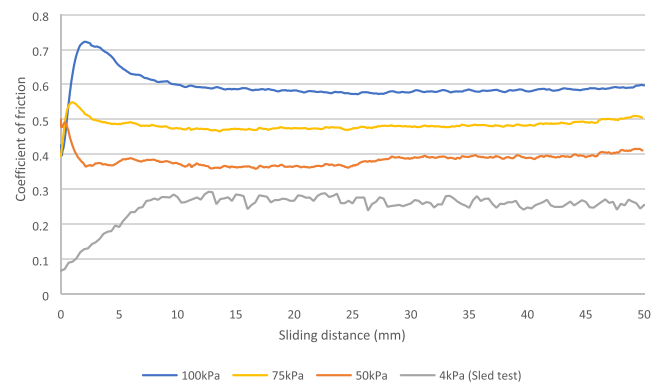


Fig. 7. Variation in the coefficient of friction of a $[-45^\circ/-45^\circ]$ surface interaction over a 50 mm sliding distance for 4 different applied pressures.

the applied normal pressure increases from 4 kPa to 100 kPa. These values are significantly larger than those reported in the literature (0.18 to 0.3 [7,31,32]), which are commonly used as input parameters for forming simulations for similar materials.

Higher values for the coefficient of friction can be attributed to the deformability of the fabric plies using this approach, as an increase in applied load causes a reduction in ply thickness and a subsequent flattening of the yarns [33,34]. The change in surface topography of the fabric causes an increase in the number of asperities in contact with one another [35], increasing the real contact area between the plies. In addition, yarns and individual fibres from each ply can become nested together (commingled) for certain ply layups, further enlarging the apparent contact area.

3.2. Effect of ply stacking sequence

Fig. 8 shows contour plots for the static (left) and dynamic (right)

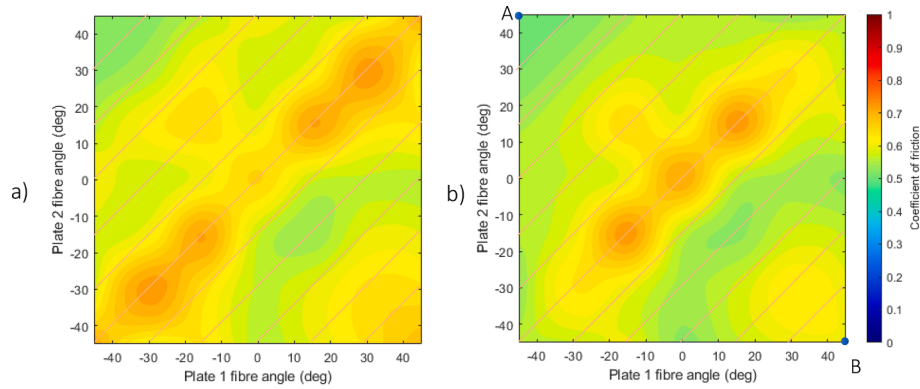


Fig. 8. Contour plots of coefficients of friction as determined from the overlap test at vacuum pressure. (a) Static coefficients of friction. (b) Dynamic coefficients of friction. Diagonal lines have been added to each plot to highlight the trend in coefficients with parallel fibre angles, and additional data points have been determined using linear interpolation to smooth the contour plot.

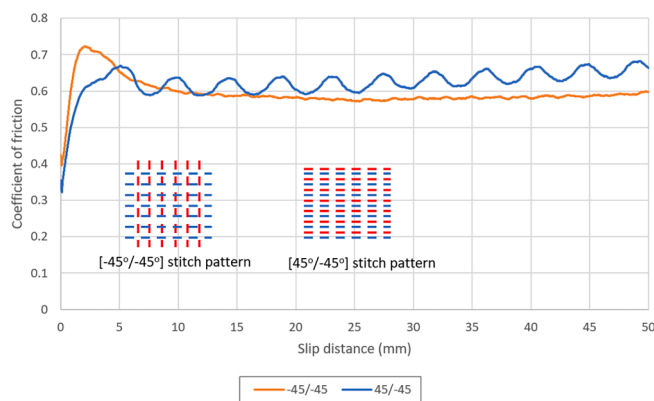


Fig. 9. A comparison of the variation in coefficient of friction for a $[-45^\circ/-45^\circ]$ surface interaction and a $[45^\circ/-45^\circ]$ surface interaction. Large oscillations in the coefficients produced by the $[45^\circ/-45^\circ]$ interaction are a result of perpendicular stitch interference, as demonstrated in shown stitch patterns.

coefficients of friction, where each axis of the plot corresponds to the fibre angle of each ply relative to the slip direction. The contour colours refer to the magnitude of the coefficient of friction. Each orientation pairing was repeated at least 3 times with new fabric samples applied for each repeat. Both plots are diagonally symmetric, as mirrored test configurations (i.e., $[0^\circ/15^\circ]$ and $[15^\circ/0^\circ]$) produced consistent coefficient of friction values within 4 %.

The observed trend is similar for both the static and dynamic coefficients of friction. It is also apparent that the range of friction coefficients produced as a result of varying the fibre orientations under a full vacuum load is smaller than those produced by varying the applied pressure (Fig. 10), indicating that ply orientation is less significant than the applied compaction pressure. The static coefficient of friction ranged from 0.521 with a $[-45^\circ/45^\circ]$ interaction, to 0.731 at a $[-30^\circ/-30^\circ]$ interaction. Similarly, the dynamic coefficient range started at 0.500 for a $[-45^\circ/45^\circ]$ interaction and increased up to a maximum value of 0.732 at $[-15^\circ/-15^\circ]$. Peak coefficients for both static and dynamic friction were observed where inter-ply fibres were parallel and stitches were perpendicular. Diagonal lines have been added to the contour plots in Fig. 8 to highlight this trend. Coefficients at orientations other than 0° were observed to be less dependent on inter-ply fibre angle, producing a more uniform coefficient distribution, with the exception of $[45^\circ/-45^\circ]$, which produced a higher static coefficient due to parallel stitches at the interface.

Fibre orientations where the inter-ply fibre angles were the same, but the stitch angles were different, did not produce the same coefficients of friction. For example, $[45^\circ/-45^\circ]$ with a $90^\circ/-90^\circ$ stitch angle pairing

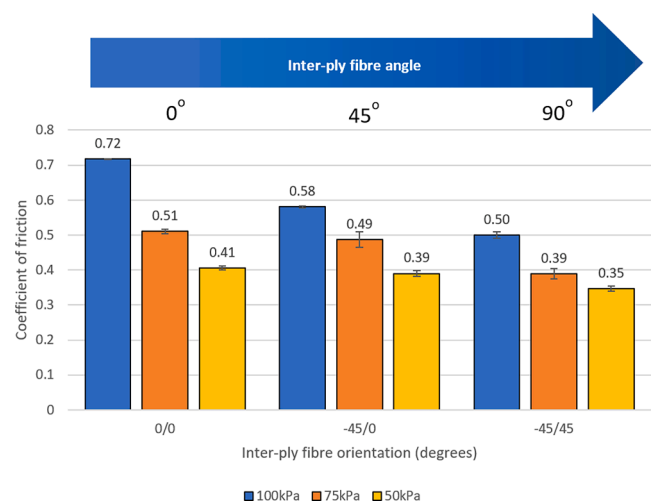


Fig. 10. Variation in dynamic coefficient of friction for 3 surface interaction orientations over 3 applied pressures. Error bars displayed indicate ± 1 standard deviation. The relative inter-ply fibre angle increases from left to right.

(see Point A on Fig. 8b) produced a dynamic coefficient of 0.617, and $[-45^\circ/45^\circ]$ with a $0^\circ/0^\circ$ stitch angle pairing (see Point B on Fig. 8b) produced a dynamic coefficient of 0.500. Whilst the inter-ply fibre angle has a dominant effect on the fabric-fabric friction, the stitch angle also contributes to the sliding behaviour for this fabric.

Large oscillations in frictional forces are observed when the stitch direction of both fabric surfaces is perpendicular to the direction of slip, such as for a $[45^\circ/-45^\circ]$ ply pairing. Opposing stitches are forced to slide over each other, which is also reflected in the coefficients of friction, as shown in Fig. 9. The wavelength of the oscillations agrees closely with the pitch between the rows of stitches (4.5 mm) when both plies are perpendicular to the direction of slip. This is similar to the ‘shock phenomenon’ that has been observed during inter-ply sliding of plain weave fabrics [36]. Oscillations were also observed for additional orientation pairs with parallel stitch angles, such as $[0^\circ/90^\circ]$ ($45^\circ/45^\circ$ stitch interaction), with the wavelength of the oscillations increasing as the stitch angle approached 0° . The amplitude of the oscillations was observed to decrease over the course of the test when the sliding distance was greater than 50 mm, due to a reduction in the number of stitch interactions within the overlap area.

3.3. Interaction between fibre orientation and normal load

Fig. 10 shows the interaction between the applied normal pressure

and the relative fibre angle, in terms of the dynamic coefficient of friction measured by the overlap test. The influence of the fibre angle is relatively small at low applied pressures (50 kPa), as the coefficient of friction is reduced by 17 %, from 0.41 to 0.35, as the relative inter-ply angle is increased from 0° (parallel fibres) to 90° (orthogonal fibres).

The influence of the relative inter-ply angle becomes more significant as the applied normal pressure increases (i.e., at 100 kPa). The dynamic coefficient of friction reduces by 30 %, from 0.72 to 0.5, as the relative fibre angle is increased from 0° (parallel fibres) to 90° (perpendicular fibres). This reduction is caused by the nesting behaviour of the fabric, as the fibre-to-fibre contact area at the mesoscale (tow level) decreases for larger relative fibre angles (i.e., perpendicular fibres). The highest levels of fibre nesting occur between plies when the fibres on both sides of the interface are parallel (an inter-ply fibre angle of 0°), as shown in Fig. 11.

Micrographs indicate that the laminate with perpendicular fibres at the interface ($[0^\circ/90^\circ]_8$) exhibits minimal intra-ply deformation through the cross section, with the yarn shapes and spacings remaining consistent throughout. Conversely, large deformations of the ply surface can be observed when the fibres are parallel at the inter-ply interface (see Fig. 11b for $[0/90/90/0]_4$ laminate). Yarns from each ply are forced into the available gaps between the yarns of the contacting ply, deforming the fabric at the mesoscale. Individual fibres from different plies become commingled, dramatically changing the surface topography of the plies. This deformation contributes to the change in inter-ply friction in both the longitudinal and transverse slip directions. For slip in the longitudinal fibre direction, the contact area between the plies is increased as additional yarns and fibres are pushed against each other. Transverse slip is impeded by yarn deformation, as nested yarns and fibres must shear or deform during the test for the plies to move relative to one another. Similar behaviour has been observed for woven fabrics [37]. As a result of these two independent slip restriction mechanisms, any fabric-fabric surface interaction with parallel fibres will exhibit larger coefficients of friction when under load than perpendicular fibres, regardless of the relative angle of the fibres to the direction of slip.

Through-thickness fabric compaction testing can be used to quantify

the effects of fibre nesting. Compaction test results for FCIM359 can be seen in Fig. 12. Parallel fibre interactions exhibit a lower compaction stiffness than non-parallel fibre interactions, which can be attributed to the microscale nesting behaviour of the filaments. At parallel inter-ply fibre orientations (0°), yarns and individual fibres of contacting plies can slide past one another in the through-thickness direction, and therefore a higher fibre volume fraction is achieved for a given compaction pressure. If the inter-ply fibre orientation is anything other than 0° however, this nesting is inhibited, as the fibres from opposing plies prevent one another from commingling. This can be seen in Fig. 12, as the perpendicular (90°) and 45° fibre orientation interactions exhibit very similar compaction behaviour.

This compaction orientation dependency aligns closely with the results seen in the overlap friction test. A larger coefficient of friction is measured when the inter-ply fibre orientation is at 0°, due to the relatively large contact areas from increased fibre nesting along the length of the fibres. For all other inter-ply angles the nesting behaviour is reduced, as the tows only make local contact with one another at common high points along the length of the fibres, yielding lower, more uniform coefficients of friction. Imaging techniques, such as μ -CT scanning, can be used to further understand these interaction mechanisms, by capturing deformations at the *meso*-/micro level that contribute to the macro-scale compaction and friction behaviours.

3.4. Effect of slip direction

The effect of slip direction relative the global fibre direction has been studied. The frictional behaviour has been investigated for cases where the relative fibre angle at the inter-ply interface were the same (i.e., parallel fibres), but the loading direction was varied relative to the fibre direction. Thus, the slip direction varied by the same angle for both fibre directions at the interface respectively. All samples were subjected to a normal pressure of 0.1 MPa.

Fig. 13 shows the effect of slip direction on the static and dynamic inter-ply coefficients of friction. As the angle between the fibre orientation and the slip direction increases, the dynamic coefficient of friction

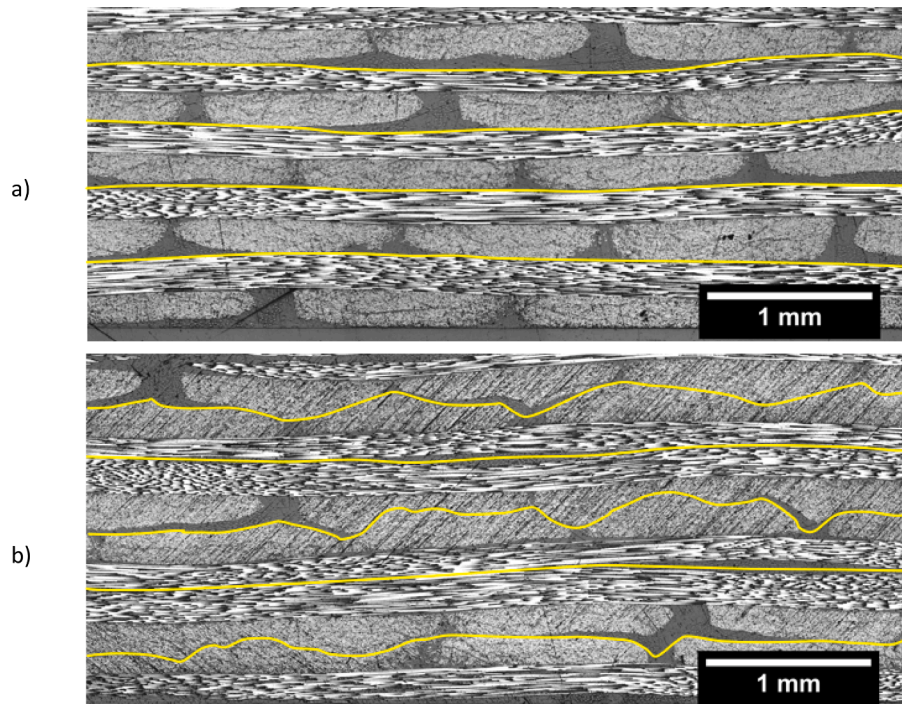


Fig. 11. (a) Optical micrograph of a $[0/90]_8$ laminate under vacuum load showing consistent yarn shape and spacing. (b) Optical micrograph of a $[0/90/90/0]_4$ laminate under vacuum load showing yarn deformation along the parallel fibre interfaces between plies. Yellow lines indicate ply interfaces. (For interpretation of the references to colour in this figure legend, the reader is referred to the web version of this article.)

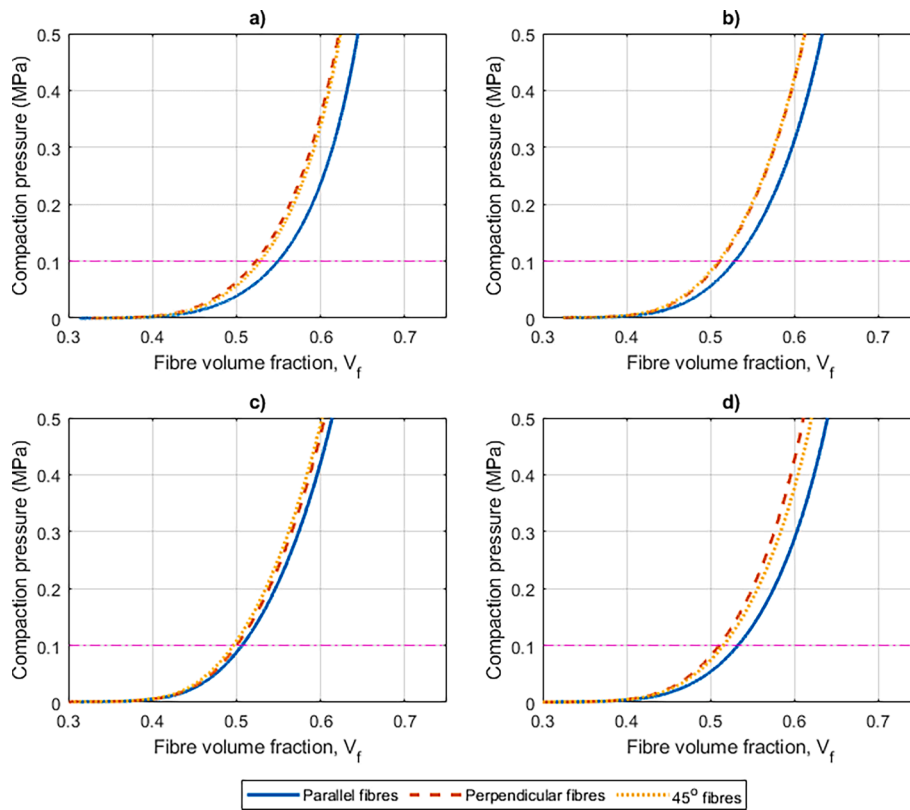


Fig. 12. Fibre volume fraction versus compaction pressure of FCIM359 laminates. (a) 10 ply laminates. (b) 8 ply laminates. (c) 4 ply laminates. (d) 2 ply laminates. Each curve represents an average of 3 repeats, and the horizontal magenta line indicates vacuum pressure, representative of a DDF process. (For interpretation of the references to colour in this figure legend, the reader is referred to the web version of this article.)

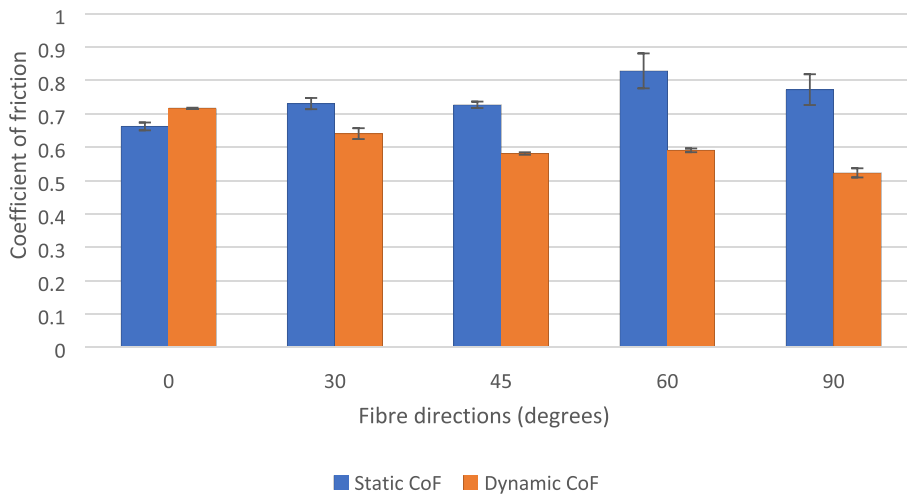


Fig. 13. Effect of slip direction on inter-ply static and dynamic coefficients of friction. Error bars show ± 1 standard deviation from the average.

decreases, while the static coefficient increases. When the fibre orientation is perpendicular to the direction of slip (transverse fibre slip), fibres must roll over one another across the radial direction, creating a large initial resistance to motion and producing a high static coefficient of friction. When in motion, however, the fibres are not able to nest as effectively, reducing the real contact area between plies and therefore reducing the dynamic coefficient of friction.

This phenomenon is also captured by the variation in the decay constants between the static to dynamic coefficients of friction (see Equation 1 for definition), as shown in Fig. 14. As the fibre orientations become perpendicular to that of the slip direction, the decay constant

increases (i.e., the sliding distance required to achieve a linear coefficient of friction decreases). The decay constant is negative when the fibre orientation and slip direction are parallel (0°), as the static coefficient of friction was determined to be lower than the dynamic coefficient in this case. This behaviour is interesting from a surface interaction modelling point of view, as it is questionable whether the static coefficient of friction is more relevant than the dynamic coefficient of friction when the inter-ply slip distances are low.

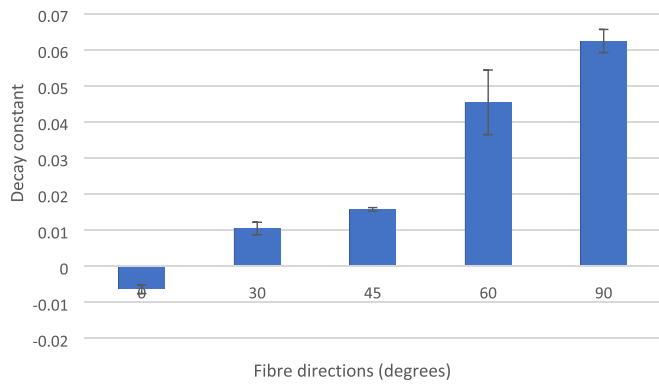


Fig. 14. Effect of slip direction on the decay constant of static to dynamic coefficients of friction. Error bars show ± 1 standard deviation from the average.

3.5. Effect of inter-laminar toughening veil

Fig. 15 shows a comparison of the dynamic coefficients of friction obtained using the overlap test for both FCIM359 and MBB00 NCFs. The FCIM359 plies exhibited a 28.8 % difference in dynamic coefficient of friction between the parallel and perpendicular fibre interactions, but the same orientations for the MBB00 NCF produced a much smaller difference of 10.9 %. The coefficients for the MBB00 (0.49 – 0.52) are both similar to the perpendicular value for the FCIM359 (0.55), as the veil prevents nesting of the fibres between plies.

Fig. 16 shows optical microscope images of two 8 ply laminates constructed using the MBB00 NCF containing the non-woven veil, which are directly comparable to the micrographs in **Fig. 11** for the FCIM359 material. Inclusion of the polymer veil between the plies clearly reduces the penetration of fibres across the inter-ply interface for the parallel MBB00 fibre orientation case, as can be seen in **Fig. 16b**, compared with the equivalent FCIM359 laminate (**Fig. 11b**).

Further compaction tests conducted with the MBB00 fabric show that inclusion of the veil material significantly reduced the orientation dependency of the compaction behaviour. **Fig. 17a, b and c** show the compaction curves for 10, 8 and 4 ply layups of MBB00 NCF respectively, with plies orientated to generate parallel (0°), perpendicular (90°) and 45° fibre orientations at every inter-ply interface. The difference in compaction stiffness between layups is minimal, agreeing closely with the optical microscopy and further indicating that inclusion of a polymer veil reduces nesting.

When compared directly to the compaction curves for the FCIM359,

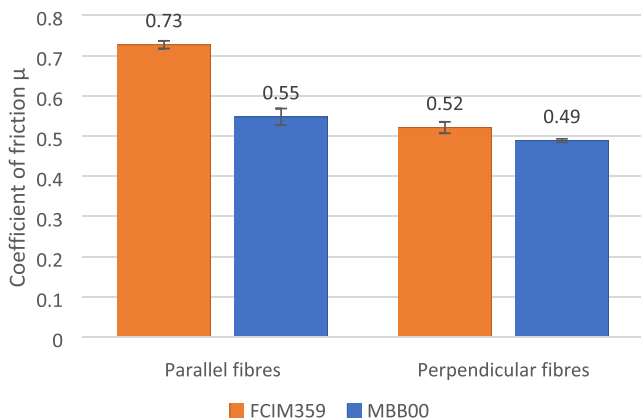


Fig. 15. Comparison of dynamic coefficients of friction for a biaxial NCF (FCIM359) and a biaxial NCF with a non-woven veil (MBB00), for both parallel and perpendicular fibre orientations. The error bars shown display ± 1 standard deviation.

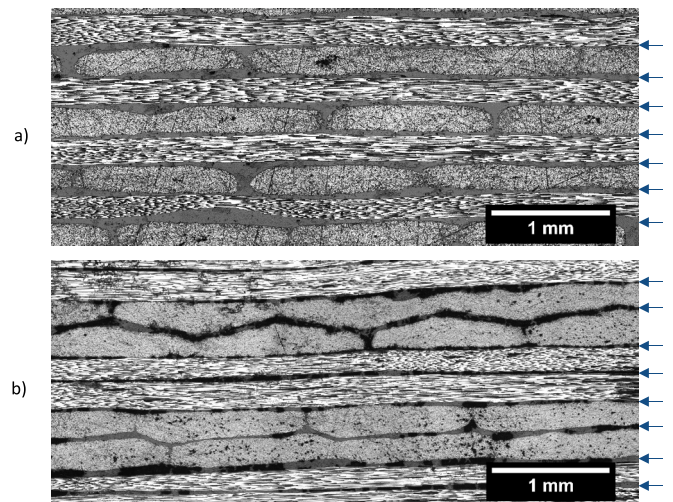


Fig. 16. Optical micrographs of 8 ply laminates with interleaved polymer veil under vacuum load. (a) $[0/90]_8$ laminate. (b) $[0/90//90/0]_4$ laminate. Arrows to the right indicate the locations for the polymer veil between each MBB00 ply.

the effect of the reduced nesting is clear. **Fig. 17d** shows the difference in compaction behaviour between the 10 ply MBB00 and FCIM359 laminates. Whilst the MBB00 material exhibits slightly stiffer compaction behaviour because of the inclusion of the veil, the orientation dependency is negligible compared to that of the FCIM359 plies. All three curves for the MBB00 samples lie on top of one another, indicating that the compaction behaviour is independent from the inter-ply fibre orientations. **Fig. 18** shows a comparison of the fibre volume fractions of the laminates when subjected to a 0.1 MPa compaction load, representative of the vacuum pressure used in the overlap test and DDF processes. The largest difference in V_f between the parallel and non-parallel fibre orientations for the FCIM359 fabric was 0.021 (3.8 %), compared with 0.002 (0.43 %) for the MBB00 material, due to the reduced fabric nesting.

Reducing inter-ply fibre nesting via the addition of a non-woven veil not only reduces the orientation dependency of the compaction behaviour, but also the orientation dependency of the inter-ply friction.

Fig. 19 shows the deformation of the veiled material as a result of the overlap test. The veil is initially distributed uniformly over the surface of the sample, but becomes distorted following during the test, as the plies experience 50 mm of slip whilst held under vacuum pressure. The veil becomes distorted by the raised stitches, causing the non-woven material to tear and agglomerate. In addition, some damage to the carbon tows was observed below the veil. As the primary purpose of the veil is to improve the inter-lamina fracture toughness, it may be important to consider how this damage influences the final mechanical performance of the component if large slip distances are required during forming.

3.6. Significance of friction on the formability of biaxial NCFs

In general, friction, shear, bending and tensile deformation mechanisms all contribute to forming behaviour. To highlight the contribution of the friction and to analyse the effect of the fibre orientation dependency, a hemisphere forming case was designed to induce controlled levels of inter-ply slip. Three of the layups used during the overlap friction test were selected to investigate the influence of the local coefficient of variation on the magnitude of the frictional forces generated during forming. Two of the configurations used fabric plies fixed to friction plates (see **Fig. 6a**) to create fabric-fabric interfaces of perpendicular and parallel fibres respectively. A simplified distribution of the initial local coefficients of friction produced by these layups can be seen in **Fig. 20**. This illustration only considers the coefficients of friction prior to any sliding or shearing of the fabric blank, as the fabric structure

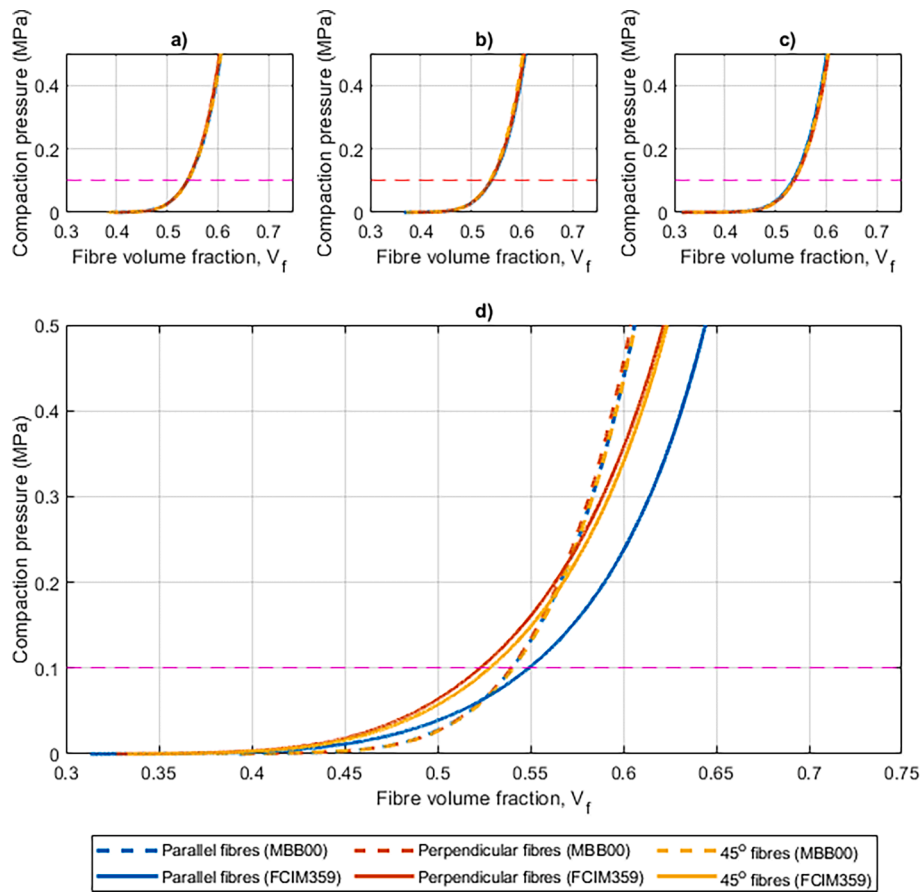


Fig. 17. (a) 10 ply MBB00 laminate compaction curves. (b) 8 ply MBB00 laminate compaction curves. (c) 4 ply MBB00 laminate compaction curves. (d) Comparison of 10 ply compaction curves for MBB00 and FCIM359 NCFs. Each curve represents an average of 3 repeats, and the horizontal magenta lines indicate vacuum pressure, representative of a DDF process. (For interpretation of the references to colour in this figure legend, the reader is referred to the web version of this article.)

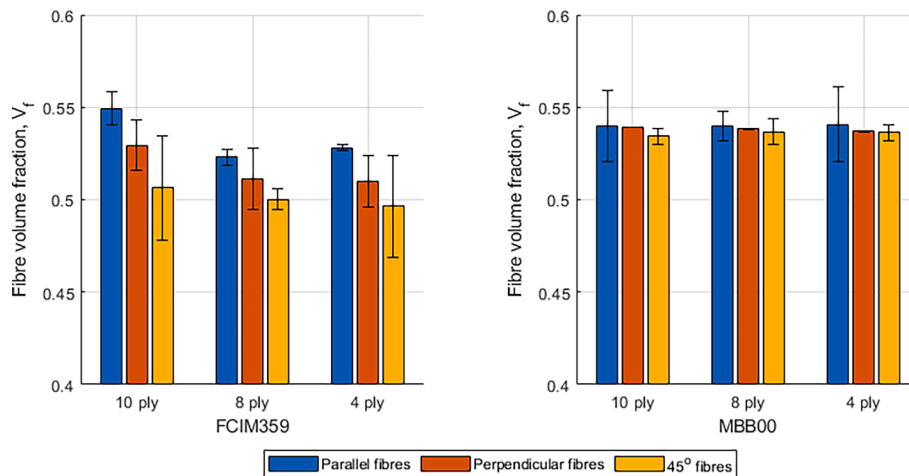


Fig. 18. Comparison of fibre volume fractions of laminates of FCIM359 and MBB00 under equivalent vacuum pressure (0.1 MPa). Error bars represent ± 1 standard deviation from the mean V_f value.

is known to change locally during forming. Slip generated at the perpendicular fibre interfaces in Fig. 20a was expected to produce a low, uniform frictional force due to the consistent orthogonal fibre arrangement between plies. According to Section 3.2, the coefficient of friction (μ_1) for this case was expected to be ~ 0.5 for full vacuum clamping pressure (0.1 MPa).

The parallel interfaces highlighted in red and blue in Fig. 20b were expected to produce higher frictional forces than the perpendicular fibre

case. Whilst the interface fibres are generally parallel, the slip direction differs between the red and blue regions. According to the results from the overlap friction test in Section 3.2, the coefficients of friction are similar for μ_2 (slip in the transverse fibre direction) and μ_1 (a perpendicular fibre interaction) at approximately 0.5. μ_3 , however, was estimated to be closer to 0.72, as per the results of the overlap test.

The third configuration used only the polished aluminium friction plates, offering a surface with a low coefficient of friction at the interface

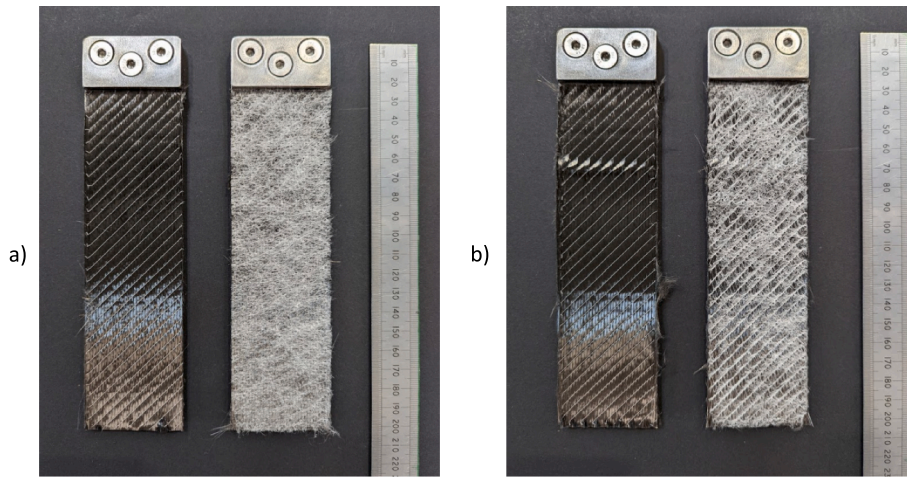


Fig. 19. (a) MBB00 NCF samples before overlap test and (b) after overlap test.

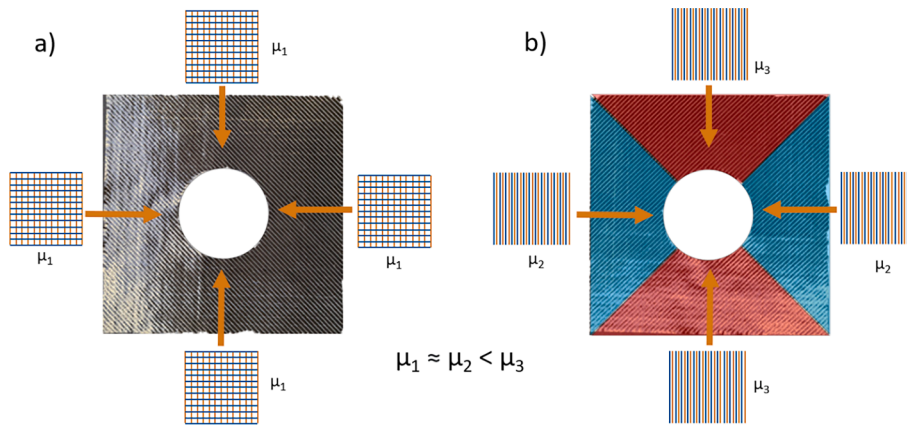


Fig. 20. Simplified diagram describing the initial distribution of local coefficients of friction prior to forming, generated by (a) perpendicular fibres and (b) parallel fibres.

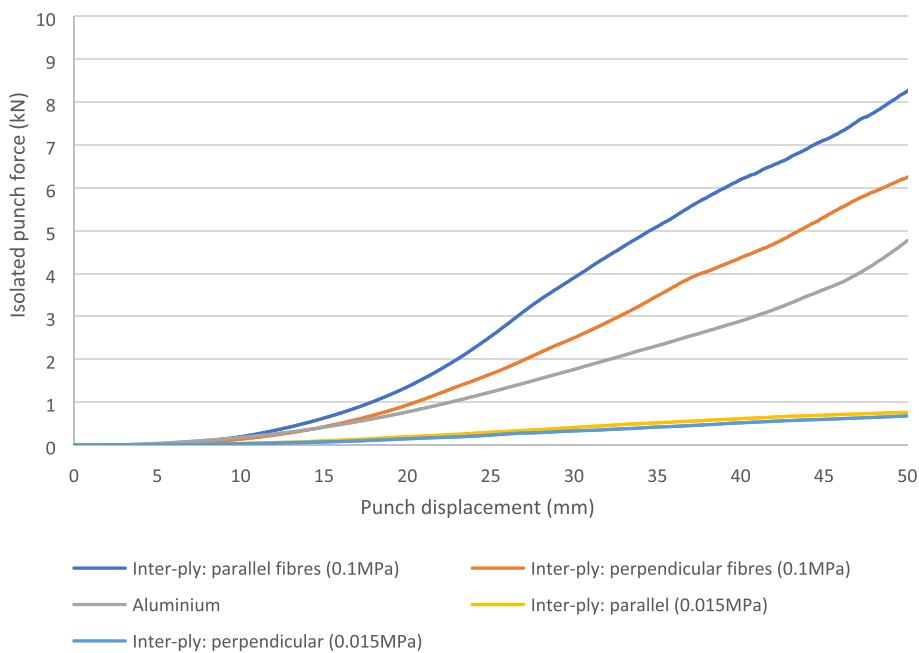


Fig. 21. Frictional force vs punch displacement results for hemisphere study.

(approximately 0.23, as determined by the sled test [38]), which served as a benchmark.

The required punch force to create the preform at the end of the 50 mm stroke was chosen as the dependent variable to assess the formability of each test set up. A higher punch force indicates lower fabric formability, which can be problematic for processes such as DDF, where forming forces are often limited. If the frictional forces in the system outweigh the forming forces, then fabric draw in will be limited and bridging can occur.

Results from the hemisphere forming study in Fig. 21 indicate that the measured punch force had a high dependency on the applied clamping pressure, with the peak force increasing from 0.75kN to 8.2kN as the applied pressure on the friction plate was increased from 0.015 MPa to 0.1 MPa.

Similar to the findings from the overlap friction test, the influence of the fibre orientations at the slip interface was less significant in terms of the forming force, but a trend could be established. Fig. 21 shows that the punch force was higher when all fibres were parallel at the inter-ply interface between the blank and the fibres attached to the friction plate, compared with the perpendicular fibre case. This difference is more significant when a full vacuum pressure is applied, which is also in agreement with the results from the overlap test. The punch force required to form the preform increases from 6.3kN to 8.2kN when the fibres are rotated at the inter-ply interface to become parallel with one another.

In addition to variations in measured punch force, anisotropic friction behaviour resulted in some additional forming defects on the surfaces of the preform. Fig. 22 shows an example of some in-plane fibre distortion, caused by failure of the stitches. This laddering phenomenon is only observed where parallel fibres at the interface slip transversely relative to one another (i.e. the blue shaded areas in Fig. 20b). As the transient fibres on the blank fibre draw in to form the hemisphere, the stationary fibres attached to the friction plate try to resist the motion, resulting in local bunching of the primary yarns and large tensile stresses in the stitches. This is indicative of the different slip mechanisms that occur during transverse slip of parallel fibres and longitudinal slip of parallel fibres, as this type of defect is not visible in the other quadrants (shaded blue in Fig. 20b).

4. Conclusions

The influence of applied pressure and ply orientation on the inter-ply frictional behaviour of NCF surface interactions has been investigated via a novel experimental method. Results have shown that coefficients of friction commonly used for DDF forming simulations are much lower than real-world values, due to the assumption that the fabric plies are non-deformable. Increasing the applied normal pressure during the overlap test from 25 kPa to 100 kPa increased the measured coefficient of friction by up to 43 %, due to increased ply-ply nesting and fabric deformation.

The anisotropic nature of fabric-fabric friction was demonstrated when surface interactions involving parallel fibres (0) produced much higher coefficients than interactions involving larger relative inter-ply fibre angles (i.e., tending to 90). This was attributed to the fabric nesting being highly dependent on fibre orientation, which was confirmed with optical microscopy and through-thickness compaction data. Inclusion of a non-woven veil material at the inter-laminar interface reduced the fibre nesting, and consequently reduced the orientation dependency of the inter-ply friction. The observed frictional behaviour and data gathered by the overlap test may be used to construct more realistic friction models. Key data points, such as decay rate, and the static and dynamic coefficients of friction (and their respective pressure and orientation dependencies) can be used to construct a constitutive surface interaction model with improved accuracy compared to existing Coulomb-based simulations.

The significance of the variation of friction was evaluated using a



Fig. 22. In-plane fibre distortion, laddering, caused by anisotropic friction in the forming process.

matched tool forming test to induce controlled inter-ply sliding. It was found that inter-ply sliding of fabric-fabric interfaces with parallel fibres required significantly higher punch forces to create a preform, and hence these architectures have lower formability and should be avoided from a Design for Manufacture point of view.

CRediT authorship contribution statement

G.D. Lawrence: Conceptualization, Methodology, Validation, Investigation, Writing – original draft. **S. Chen:** Supervision, Conceptualization, Writing – original draft. **N.A. Warrior:** Writing – review & editing. **L.T. Harper:** Conceptualization, Supervision, Writing – review & editing, Funding acquisition.

Declaration of Competing Interest

The authors declare that they have no known competing financial interests or personal relationships that could have appeared to influence the work reported in this paper.

Data availability

Data will be made available on request.

Acknowledgements

This work was funded by the Engineering and Physical Sciences Research Council [Grant number: EP/P006701/1], as part of the “EPSRC Future Composites Manufacturing Research Hub”.

References

- [1] Chen S, McGregor OPL, Endruweit A, Elsmore MT, De Focatiis DSA, Harper LT, et al. Double diaphragm forming simulation for complex composite structures. *Compos Part A Appl Sci Manuf* [Internet] 2017;95:346–58.
- [2] Thompson AJ, Belnoue JPH, Hallett SR. Modelling defect formation in textiles during the double diaphragm forming process. *Compos Part B Eng* [Internet] 2020;202(July):108357.
- [3] Hou M. Stamp forming of continuous glass fibre reinforced polypropylene. *Compos Part A Appl Sci Manuf* 1997;28(8):695–702.
- [4] Mukhopadhyay S, Jones MI, Hallett SR. Tensile failure of laminates containing an embedded wrinkle; numerical and experimental study. *Compos Part A Appl Sci Manuf* 2015;77:219–28.
- [5] Mukhopadhyay S, Jones MI, Hallett SR. Compressive failure of laminates containing an embedded wrinkle; Experimental and numerical study. *Compos Part A Appl Sci Manuf* [Internet] 2015;73:132–42.
- [6] Sharma SB, Sutcliffe MPF, Chang SH. Characterisation of material properties for draping of dry woven composite material. *Compos Part A Appl Sci Manuf* 2003;34(12):1167–75.

- [7] Boisse P, Hamila N, Vidal-Sallé E, Dumont F. Simulation of wrinkling during textile composite reinforcement forming. Influence of tensile, in-plane shear and bending stiffnesses. *Compos Sci Technol* [Internet] 2011;71(5):683–92.
- [8] Hallander P, Akermo M, Mattei C, Petersson M, Nyman T. An experimental study of mechanisms behind wrinkle development during forming of composite laminates. *Compos Part A Appl Sci Manuf* [Internet] 2013;50:54–64.
- [9] Li L, Zhao Y, Vuong H, gia nam, Chen Y, Yang J, Duan Y. In-plane shear investigation of biaxial carbon non-crimp fabrics with experimental tests and finite element modeling. *Mater Des* [Internet] 2014;63:757–65.
- [10] Sourki R, Crawford B, Vaziri R, Milani AS. Orientation Dependency and Hysteresis Nature of Inter-Ply Friction in Woven Fabrics. *Appl Compos Mater* [Internet]. 2021;(0123456789).
- [11] Yu F, Chen S, Harper LT, Warrior NA. Investigation into the effects of inter-ply sliding during double diaphragm forming for multi-layered biaxial non-crimp fabrics. *Compos Part A Appl Sci Manuf* 2021;150(May).
- [12] Rashidi A, Keegan C, Milani AS. Analysis of inter-ply friction in consolidation process of thermoset woven prepregs. *AIP Conference Proceedings* 2019;2113 (July):1–7.
- [13] Rashidi A, Crawford B, Milani AS. A Mixed Lubrication Model for Inter-Ply Friction Behavior of Thermoset Prepregs. 11th Can Conf Compos 2018:1–8.
- [14] Wang W-T, Yu H, Potter K, Kim B. C. Improvement of Composite Drape Forming Quality by Enhancing Interply Slip . In ECCM17 - 17th European Conference on Composite Materials : Munich , German , 26-30 June 2016 . European Conferen. 2016;(June):26–30.
- [15] Nosrat Nezami F, Gereke T, Cherif C. Active forming manipulation of composite reinforcements for the suppression of forming defects. *Compos Part A Appl Sci Manuf* [Internet] 2017;99:94–101.
- [16] Mulvihill DM, Smerdova O, Sutcliffe MPF. Friction of carbon fibre tows. *Compos Part A Appl Sci Manuf* [Internet] 2017;93:185–98.
- [17] Tournalias M, Bueno MA, Fassi G, Aktas I, Wielhorski Y. Influence of friction angle between carbon single fibres and tows: Experimental analysis and analytical model. *Compos Part A Appl Sci Manuf* 2019;124(June).
- [18] Chakladar ND, Mandal P, Potluri P. Effects of inter-tow angle and tow size on carbon fibre friction. *Compos Part A Appl Sci Manuf* [Internet] 2014;65:115–24.
- [19] Robitaille F, Gauvin R. Compaction of textile reinforcements for composites manufacturing. I: Review of experimental results. *Polym Compos* 1998;19(2): 198–216.
- [20] Cornelissen B, Sachs U, Rietman B, Akkerman R. Dry friction characterisation of carbon fibre tow and satin weave fabric for composite applications. *Compos Part A Appl Sci Manuf* [Internet] 2014;56:127–35.
- [21] Avgoulas EI, Mulvihill DM, Endruweit A, Sutcliffe MPF, Warrior NA, De Focatis DSA, et al. Frictional behaviour of non-crimp fabrics (NCFs) in contact with a forming tool. *Tribol Int* [Internet] December 2017;2018(121):71–7.
- [22] British Standard. *Plastics — Film and sheeting — Determination of the coefficients of friction*. Vol. 3. 2004.
- [23] Drews A. *Standard Test Method for Static and Kinetic Coefficients of Friction of Plastic Film and Sheetting*. *Man Hydrocarb Anal* 6th Ed. 2008;545-545–3.
- [24] Fulleringer N, Bloch JF. Forced stick-slip oscillations allow the measurement of the friction force: Application to paper materials. *Tribol Int* [Internet] 2015;91:94–8.
- [25] Sachs U, Akkerman R, Fetfatsidis K, Vidal-Sallé E, Schumacher J, Ziegmann G, et al. Characterization of the dynamic friction of woven fabrics: Experimental methods and benchmark results. *Compos Part A Appl Sci Manuf* [Internet] 2014; 67:289–98.
- [26] Fetfatsidis KA, Jauffrès D, Sherwood JA, Chen J. Characterization of the tool/fabric and fabric/fabric friction for woven-fabric composites during the thermostamping process. *Int J Mater Form* 2013;6(2):209–21.
- [27] Gorczyca-Cole JL, Sherwood JA, Chen J. A friction model for thermostamping commingled glass-polypropylene woven fabrics. *Compos Part A Appl Sci Manuf* 2007;38(2):393–406.
- [28] Fetfatsidis KA, Gamache LM, Gorczyca JL, Sherwood JA, Jauffrès D, Chen J. Design of an apparatus for measuring tool/fabric and fabric/fabric friction of woven-fabric composites during the thermostamping process. *Int J Mater Form* 2013;6(1):1–11.
- [29] Kim JY, Hwang YT, Baek JH, Song WY, Kim HS. Study on inter-ply friction between woven and unidirectional prepregs and its effect on the composite forming process. *Compos Struct* October 2020;2021(267):113888.
- [30] Rashidi A, Montazerian H, Yesilcimen K, Milani AS. Experimental characterization of the inter-ply shear behavior of dry and prepreg woven fabrics: Significance of mixed lubrication mode during thermoset composites processing. *Compos Part A Appl Sci Manuf* [Internet]. 2020;129(November 2019):105725.
- [31] Bel S, Hamila N, Boisse P, Dumont F. Finite element model for NCF composite reinforcement preforming: Importance of inter-ply sliding. *Compos Part A Appl Sci Manuf* [Internet] 2012;43(12):2269–77.
- [32] Yu F, Chen S, Viisainen JV, Sutcliffe MPF, Harper LT, Warrior NA. A macroscale finite element approach for simulating the bending behaviour of biaxial fabrics. *Compos Sci Technol* 2020;191(January).
- [33] Chen B, Chou TW. Compaction of woven-fabric preforms in liquid composite molding processes: Single-layer deformation. *Compos Sci Technol* 1999;59(10): 1519–26.
- [34] Grieser T, Mitschang P. Investigation of the compaction behavior of carbon fiber NCF for continuous preforming processes. *Polym Compos* 2017;38(11):2609–25.
- [35] Hutchings I, Shipway P. *Friction and Wear of Engineering Materials*. Tribology: Friction and Wear of Engineering Materials; 2017.
- [36] Montero L, Allaoui S, Hivet G. Characterisation of the mesoscopic and macroscopic friction behaviours of glass plain weave reinforcement. *Compos Part A Appl Sci Manuf* [Internet] 2017;95:257–66.
- [37] Allaoui S, Hivet G, Wendling A, Ouagne P, Soulat D. Influence of the dry woven fabrics meso-structure on fabric/fabric contact behavior. *J Compos Mater* 2012;46 (6):627–39.
- [38] Chen S, McGregor OPL, Harper LT, Endruweit A, Warrior NA. Defect formation during preforming of a bi-axial non-crimp fabric with a pillar stitch pattern. *Compos Part A Appl Sci Manuf* [Internet] 2016;91:156–67.
- [39] Yu F, Chen S, Harper LT, Warrior NA. Double diaphragm forming simulation using a global-to-local modelling strategy for detailed defect detection in large structures. *Compos Part A Appl Sci Manuf* 2021;147(April).
- [40] Viisainen V, Zhou J, Sutcliffe M, Street T. Development of a Composite Forming Limit Diagram: A Feasibility Study. 22nd ICCM Int Conf Compos Mater 2019.